HEAT AND MASS TRANSFER MODELING OF VACUUM INSULATED VESSEL STORING CRYOGENIC LIQUID IN LOSS OF VACUUM ACCIDENT

Xu, Zhanjie[1], Jordan, Thomas[1], Friedrich, Andreas[1], Vagts, Steffen[2], Friese, Peter[2], Adamczyk, Anna[2]

[1]Karlsruhe Institute of Technology, P.O. Box 3640, 76021 Karlsruhe, Germany

[2]Airbus Operations GmbH, Kreetslag 10, 21129 Hamburg, Germany

ABSTRACT

Cryogenic liquid is often stored in a vacuum insulated Dewar vessel for a high efficiency of thermal insulation. Multi-layer insulation (MLI) can be further applied in the double-walled vacuum space to reduce the heat transfer from the environment to the stored cryogenic fluid. However, in loss-of-vacuum accident (LOVA) scenarios, heat flux across the MLI will raise to orders of magnitudes larger than with an intact vacuum shield. The cryogenic liquid will boil intensively and pressurize the vessel due to the heat ingress. The pressurization endangers the integrity of the vessel and poses an extra catastrophic risk if the vapor is flammable, e.g., hydrogen. Therefore, safety valves have to be designed and installed appropriately, to make sure the pressure is limited to acceptable levels. In this work, the dynamic process of the heat and mass transfers in the LOVA scenarios is studied theoretically. The mass deposition - desublimation of gaseous nitrogen on cryogenic surfaces is modeled, as it provides the dominant contribution of the thermal load to the cryogenic fluid. The conventional heat convection and radiation are modeled too, although they play only secondary roles, as realized in the course of the study. The temperature dependent thermal properties of e.g., gaseous and solid nitrogen and stainless steel are used to improve the accuracy of calculation in the cryogenic temperature range. Presented methodology enabling the computation of thermodynamic parameters in the cryogenic storage system during LOVA scenarios provides further support for the future risk assessment and safety system design.

Key Words: cryogenic liquid; vacuum insulation; multi-layer insulation (MLI); loss-of-vacuum accident (LOVA); hydrogen safety.

1 INTRODUCTION

Cryogenic condition often refers to a temperature below 120 K. Cryogenic technology can be traced back to the late 19th century and has a wide range of applications so far e.g., in medicine, aerospace, superconductor, energy storage etc. [14,15] Gas liquefaction is an important application of cryogenic technology such as preparations of liquid helium, liquid nitrogen, LNG etc.. Liquid hydrogen (LH2) is a favourite energy storage form in particular for weight critical applications with a high energy and power demand due to its high mass specific energy density and additional cooling capacity.

Double-walled Dewar containers are often used to store cryogenic liquids due to the high thermal insulation provided by the vacuum, with a typical remaining pressure of about 10^{-5} Pa between the inner and outer walls of the container. The vacuum insulation is one of the key factors to keep the cryogenic condition inside because it reduces effectively heat transfer from the environment. However, increased thermal ingress may occur in case of loss-of-vacuum accident (LOVA), which is defined as an accident scenario caused by an unintentional break of the vacuum enclosure on the vessel walls or the connected piping, or by the failure of the vacuum maintaining system etc.

In LOVA scenarios the gases breaking the vacuum raise the heat transfer and induce serious heat loads to the cryogenic liquid. The liquid will boil intensively and the generated gas pressurizes the container. The pressurization rate depends on the rupture size. The pressurization endangers the integrity of the container. A large amount of vapor may be released after the failure of the container. If the stored liquid is hydrogen, extra catastrophic risks exist due to its high flammability and detonability. To release the

vapor under control, a safety relief device [18] is indispensable for the LH2 tank, which can be activated to mitigate the potential risks in case of accidental thermal ingress like in LOVAs.

The objective of the study is to clarify the heat and mass transfer phenomenon in the double-walled vacuum space in LOVAs for a LH2 tank. The heat and mass transfer processes are modelled based on the carefully collected material properties at cryogenic temperatures [10, 13, 22-24]. The dynamic parameters of the LH2 cryostat in LOVA scenarios are estimated based on the modelling calculations. The obtained results supply a good base for further safety design of the LH2 storage system.

2 LH2 CRYOSTAT AND ANALYTICAL ASSUMPTIONS

A test facility for the investigation of LOVA events in LH2-storage vessels is designed at KIT. The schematic diagram of the experimental facility is shown in Fig. 1.

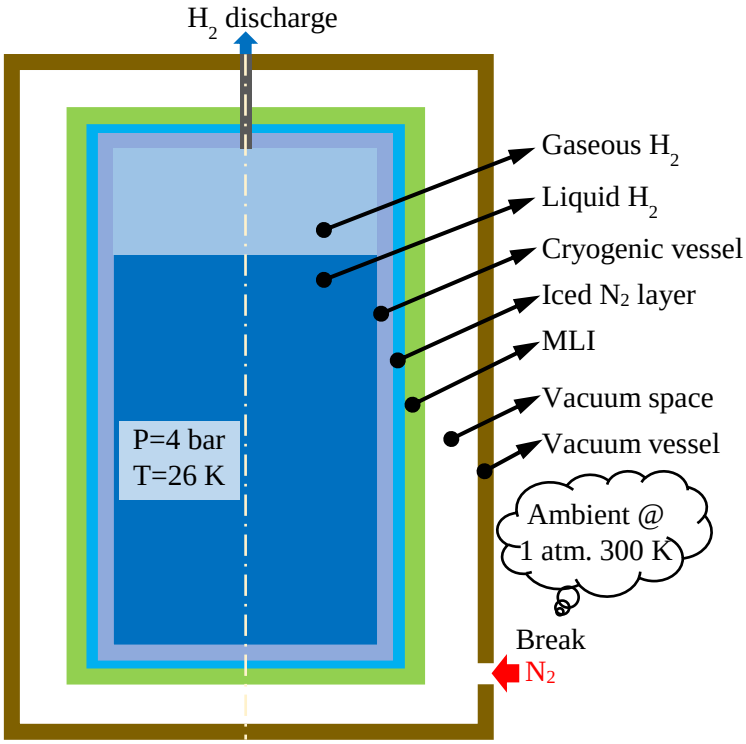

Figure 1. Scheme of the test facility for LOVAs in LH2 cryostats

As shown in Fig.1, the LH2 cryostat consists mainly of the cryogenic vessel (inner) and the vacuum vessel (outer). The inner vessel contains liquid hydrogen in 80 % of the total volume and gaseous hydrogen in 20 % at the saturation state with an absolute pressure of 4 bar and temperature of 26 K [16]. A two-phase discharge of hydrogen at the top of the cryostat has turned out to be not very efficient. Thus, LH2 is designed intentionally not to fill the complete nominal volume of the inner vessel, to guarantee only a gaseous discharge flow in demand. The outer vessel isolates the storage tank from the environment and forms the vacuum space together with the cryogenic vessel. To improve the thermal insulation, a multi-layer-insulation (MLI) system is wrapped around the cryogenic vessel, which is made of interleaving structure between reflective foils and insulating spacers [4].

Important assumptions are made as follows for the following modelling work.

- The initiator of the LOVA is assumed typically as a break on the vacuum vessel wall, as shown in Fig.1.

- Due to the unavailability of the properties of solidified air at cryogenic temperatures, the venting gas is assumed as pure nitrogen. Such a substitution may bring an error of less than 10% according to [1].

- The venting nitrogen gas experiences phase change due to the cryogenic condition on the steel wall of cryogenic vessel or even in some inner layers of the MLI. The temperature is mostly below the triple point of nitrogen. Thus, desublimation occurs while gas molecules deposit on the solid surfaces. The non-compressed structure of the MLI is not gas tight at all. The venting gas molecules can readily diffuse to the vicinity of the outer wall surface of the cryogenic vessel, which has the lowest temperature in the entire vacuum enclosure. A rational assumption is made that the nitrogen crystals are formed mostly on the steel wall. Possible deposition in the MLI structures is ignored. The solid nitrogen layer is shown in blue in Fig.1, between the cryogenic vessel and the MLI.

- The initial pressure of the cryogenic vessel and the set pressure for hydrogen discharge is equally defined as 4 bar (absolute). It means that the two-phase hydrogen in the vessel stays in saturation during the concerned time duration in the LOVA. Therefore, the temperature of LH2 is assumed as 26 K uniformly, by ignoring possibly slight stratification of temperature in the two-phase fluid.

3 KEY PHYSICAL PHENOMENA IN LOVA

3.1 Break flow model

The ambient gas enters the vacuum volume through the break once LOVA occurs. Depending on the pressure difference between the ambient and the vacuum enclosure, the venting flow can be critical or sub-critical. The mass flow rate at the break is well formulated as [1],

$$mIn(P_v) = \begin{cases} A_v(2P_a\rho_a)^{0.5}\left(\frac{2}{\kappa_a+1}\right)^{\frac{1}{\kappa_a-1}}\left(\frac{\kappa_a}{\kappa_a+1}\right)^{0.5}, if\ P_v < P_{vc} \\ A_v(2P_a\rho_a)^{0.5}\left\{\frac{\kappa_a}{\kappa_a-1}\left[\left(\frac{P_v}{P_a}\right)^{\frac{2}{\kappa_a}} - \left(\frac{P_v}{P_a}\right)^{\frac{\kappa_a+1}{\kappa_a}}\right]\right\}^{0.5}, if\ P_v \geq P_{vc} \end{cases} \quad \text{(Eq. 1)}$$

$$P_{vc} = P_a\left(\frac{2}{\kappa_a+1}\right)^{\frac{\kappa_a}{\kappa_a-1}} \quad \text{(Eq. 2)}$$

where, mIn is the mass inflow rate at the break, kg/s; P_v the pressure in the vacuum vessel, Pa; P_a the ambient pressure, Pa; ρ_a the ambient gas density, kg/m^3; A_v the break area, m^2; κ_a the specific heat ratio of the venting gas; P_{vc} the critical pressure in the vacuum vessel, Pa, which divides the venting flows into critical flow and sub-critical flow at different stages.

3.2 Loss of vacuum

The vacuum is lost gradually due to the venting flow at the break, which pressurizes the vacuum volume. On the other hand, the venting gas molecules are adhered on the cryogenic solid surface due to desublimation, as a mass sink. Therefore, according to ideal gas equation of state, the vacuum pressure follows,

$$\frac{dP_v}{dt} = \frac{T_v R_a}{V_v}\left[mIn(P_v) - A_{cr} m_{dep}(P_v, T_v, T_{cr})\right] \quad \text{(Eq. 3)}$$

where, P_v is the vacuum pressure, Pa; t, the time, s; T_v the gas temperature in the vacuum, K; R_a the venting gas constant, J/K/kg; V_v the vacuum volume, m^3; A_{cr} the cryogenic surface area for mass deposition, m^2; m_{dep} the mass deposition rate, kg/m^2/s, which depends on the vacuum pressure, temperature and the surface cryogenic temperature for desublimation.

3.3 Mass deposition model

It is not trivial to model desublimation precisely due to many factors. The mass deposition rate of venting gas is mostly measured as data by means of experiment, e.g. [32].

The phase change of the venting gas is from vapor directly to solid, if the cryogenic temperature is below the triple point of the gas. The mass deposition process is called desublimation. Or it is called condensation if the temperature is higher than the triple point. The driven potence to phase change is primarily the difference between the gas density at the bulk temperature and the saturated gas density at the solid surface temperature. The cryogenic surface "sucks" the gas molecules like a mass sink due to the so-called cryopumping effect. The mass deposition rate is modeled as,

$$m_{dep}(P_v, T_v, T_{cr}) = k_{dep}[\rho_v(P_v, T_v) - \rho_{sat}(T_{cr})] \quad \text{(Eq. 4)}$$

where, m_{dep} is the mass deposition rate on unit surface area, kg/m^2/s; ρ_v the bulk gas density at the pressure P_v and temperature T_v in the vacuum enclosure, kg/m^3; ρ_{sat} is the saturated gas density, kg/m^3, as a function of the cryogenic temperature T_{cr}; k_{dep} the mass transfer coefficient, m/s.

The determination of the mass transfer coefficient is one of the key points in the mass deposition model in the study. It can be determined experimentally, but only few data is available. The mass transfer coefficient was measured on snow sublimations by T. A. Neumann [32]. The measured data were adopted by other researchers in their modeling of nitrogen desublimation on a liquid helium cryostat [1,2] and good results were obtained, even after being verified against experimental data.

Therefore, the measured k_{dep} by T. A. Neumann is also adopted in the LH2 study. By ignoring the convection factor, the mass transfer coefficient takes a constant [32],

$$k_{dep} = 0.075 \quad \text{(Eq. 5)}$$

Accordingly, the heat flux due to mass deposition is determined as,

$$q_{dep}(P_v, T_v, T_{cr}) = m_{dep}(P_v, T_v, T_{cr})[h_v(T_v) - h_{cr}(T_{cr})] \quad \text{(Eq. 6)}$$

where, q_{dep} is the heat flux due to desublimation, W/m^2; h_v the bulk gas enthalpy at the vacuum temperature T_v, J/kg; h_{cr} the solid or liquid enthalpy of the venting gas at the cryogenic temperature T_{cr}, J/kg. The thermal load is transferred by means of conduction through the solid layers or walls into the LH2.

The generation rate of solid nitrogen is determined by,

$$\frac{dM_{sn}}{dt} = m_{dep}A_{sn} \quad \text{(Eq. 7)}$$

where, M_{sn} is the total mass of iced nitrogen, kg; A_{sn}, the surface area of the solid nitrogen layer in m^2, where desublimation takes place.

3.4 Heat transfer models

A zero-dimensional lumped parameter model is set up to analyze the heat transfer processes from the "warm" vacuum space, layer-by-layer to the MLI, to the iced nitrogen layer and the cryogenic vessel wall, finally to the cryogenic liquid hydrogen, as shown in Fig. 2. The vacuum vessel wall is not modeled for simplification. A conservative assumption is also made that the gas temperature in the vacuum enclosure is equal to the ambient temperature, i.e. $T_v = T_a$, although the T_v should be slightly lower than the T_a due to the expansion flow at the break.

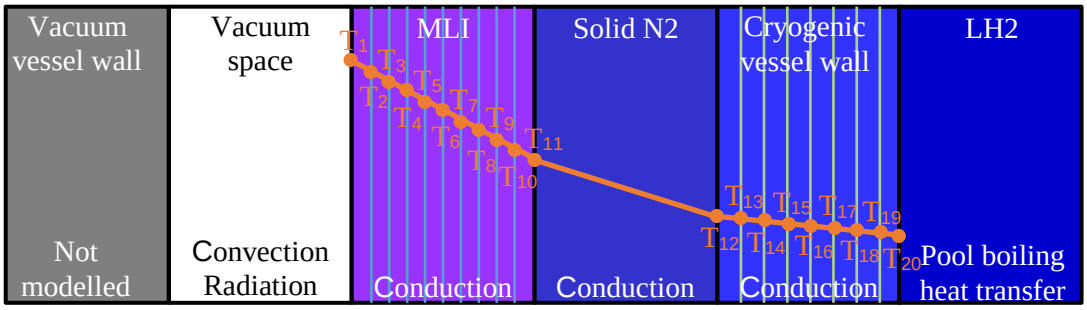

Figure 2. Lumped parameter model for heat transfer analysis with 10 nodes of MLI, 1 node of solid nitrogen layer and 8 nodes of cryogenic wall (stainless steel 316)

The 10-layer MLI system is modeled by 10 nodes, namely, modeled layer by layer. The mass deposition occurs firstly on the outer wall surface of the cryogenic vessel. Then the iced layer surface substitutes gradually the steel surface as the growing base of nitrogen crystals. The actual thickness of the iced layer is normally less than 1 mm, so it is modeled by one node. The vessel wall is represented by 8 nodes for accuracy consideration. The temperatures T_i $(i = 1,2, \dots 20)$ are the sought solutions by solving the heat transfer equations.

3.4.1 Convection

Heat transfer occurs between the venting gas and the outer surface of the MLI by natural convection in the vacuum space during LOVA. The heat transfer coefficient (HTC) and the corresponding heat flux due to convection are determined by using the following correlations [11].

$$Nu = \begin{cases} 0.197Ra^{0.25}\left(\frac{L}{\mathrm{H}}\right)^{\frac{1}{9}}, if\ \mathrm{Ra} < 2 \cdot 10^5 \\ 0.073Ra^{\frac{1}{3}}\left(\frac{L}{\mathrm{H}}\right)^{\frac{1}{9}}, if\ \mathrm{Ra} \geq 2 \cdot 10^5 \end{cases} \quad \text{(Eq. 8)}$$

$$\alpha = \frac{Nu \cdot k_{N2}}{L} \quad \text{(Eq. 9)}$$

$$q_{conv} = \alpha(T_v - T_1) \quad \text{(Eq. 10)}$$

where, Nu is the Nusselt number; Ra the Rayleigh number with respect to gaseous nitrogen; L the gap width of the vacuum enclosure, m; H the height of the vacuum, m; α the heat transfer coefficient, W/m^2/K; k_{N2} the thermal conductivity of gaseous nitrogen, W/m/K; q_{conv} the heat flux due to convection, W/m^2; T_1 the temperature of the outer surface of MLI, K.

3.4.2 Thermal radiation

Heat exchange exists between the inner wall of the vacuum vessel and the outer surface of MLI due to thermal radiations. The heat flux is determined by the Stefan-Boltzmann law for the concentric annular geometry [3].

$$q_{rad} = \frac{\sigma\left(T_v^4 - T_1^4\right)}{\frac{1}{\epsilon_{ss}} + \frac{A_{ss}}{A_{al}}\left(\frac{1}{\epsilon_{al}} - 1\right)} \quad \text{(Eq. 11)}$$

where, q_{rad} is the heat flux due to thermal radiation, W/m^2; σ the Stefan-Boltzmann constant $5.67 \cdot 10^{-8}$ W/m^2/K^4; A_{ss} the inner surface area of the vacuum vessel (stainless steel), m^2; A_{al}, the outer surface area of the MLI (aluminium), m^2; ϵ_{ss} and ϵ_{al} are the emissivities of the stainless steel and aluminium surfaces, respectively [19-21].

3.4.3 Pool boiling heat transfer

The saturated liquid hydrogen in the cryogenic vessel boils, if it is heated by the vessel wall in case of LOVA. The boiling heat transfer can be determined by using correlations for different regimes of boiling [5-8,17]. The Kutateladze correlation for pool boiling heat transfer [5], which has been verified for cryogenic fluids including N2, O2, H2, and He, is adopted hereby,

$$q_{boil}(T_w) = \mu_f H_{fg} \left[\frac{g(\rho_f-\rho_g)}{\sigma_f}\right]^{0.5} \left[\frac{Kp^{0.7} Cp_f (T_w-T_s)}{881 Pr_f^{0.65} H_{fg}}\right]^{\frac{10}{3}} \quad \text{(Eq. 12)}$$

$$Kp = \frac{\rho_f P_s}{\rho_g [g\sigma_f(\rho_f-\rho_g)]^{0.5}} \quad \text{(Eq. 13)}$$

where, q_{boil} is the heat flux due to bulk boiling, W/m^2; μ_f the dynamic viscosity of LH2, Pa·s; H_{fg} the latent heat of vaporization of LH2, J/kg; g the gravity, m/s^2; ρ_f the LH2 density, kg/m^3; ρ_g the gaseous hydrogen density, kg/m^3; σ_f the surface tension of LH2, N/m; Cp_f the specific heat capacity of LH2, J/kg/K; Pr_f the Prandtl number of LH2; T_w the vessel wall temperature, K; T_s the saturation temperature of LH2, K; Kp a dimensionless quantity; P_s the saturation pressure of hydrogen vapor, Pa.

3.4.4 Thermal conduction

The thermal conduction effect of the MLI, the solid nitrogen layer and the steel wall can be modeled by their thermal resistances. The temperature dependency of the material properties is considered in the model due to their significant change in the considered temperature range.

(i) MLI is widely used in cryogenic applications. Modelling on the insulation mechanism of the MLI is conducted, e.g. in [4, 9, 12]. However, an apparent thermal conductivity of the MLI is measured by the manufacturer, which varies on the vacuum pressure and the local temperature in the MLI. The thermal insulance (R-value) of one layer of insulation is formulated as,

$$R_{ins}(P_v, T_{ins}) = \frac{th_{ins}}{k_{ins}(P_v, T_{ins})} \quad \text{(Eq. 14)}$$

where, R_{ins} is the thermal insulance of one layer of insulation material, m^{2}K/W; th_{ins} the layer thickness, m; k_{ins} the measured thermal conductivity, W/m/K, which is a function of the vacuum pressure P_v and the layer temperature T_{ins}. In mathematical practice, for each node, the layer temperature can be approximated by the average value, i.e. $T_{ins} = (T_i + T_{i+1})/2$, (i = 1,2, ... 10) for the ith node by referring to Fig. 2.

(ii) The thermal insulance of the solid nitrogen layer is formulated as,

$$R_{sn}(M_{sn}, T_{sn}) = \frac{th_{sn}(M_{sn}, T_{sn})}{k_{sn}(T_{sn})} \quad \text{(Eq. 15)}$$

$$th_{sn}(M_{sn}, T_{sn}) = \frac{M_{sn}}{\rho_{sn}(T_{sn}) A_{sn}} \quad \text{(Eq. 16)}$$

where, R_{sn} is the thermal insulance of solid nitrogen layer, m^{2}K/W; th_{sn} the solid layer thickness, m; k_{sn} the thermal conductivity of solid nitrogen, W/m/K, which is strongly depending on its temperature T_{sn}; M_{sn} the total deposited mass, kg; ρ_{sn} the density of solid nitrogen, kg/m^3, which varies significantly on its temperature.

The temperature of the solid nitrogen layer can be approximated by the average, i.e. $T_{sn} = (T_{11} + T_{12})/2$, by referring to Fig. 2. In the layer thickness calculation (Eq. 16), the actual cylindrical annular geometry of the layer is approximated by a thin plane, because the ratio of the thickness over the diameter is in an order of 10^{-3} in practice [1].

(iii) The thermal insulance of the cryogenic vessel wall (stainless steel) is simply formulated as,

$$R_{ss}(T_{ss}) = \frac{th_{ss}}{k_{ss}(T_{ss})} \quad \text{(Eq. 17)}$$

where, R_{ss} is the thermal insulance of stainless steel, m^{2}K/W; th_{ss} the steel thickness, m; k_{ss} the thermal conductivity of steel, W/m/K, which varies on its temperature T_{ss} in the cryogenic condition.

4 GOVERNING EQUATIONS

According to the Fourier's law, 19 heat conduction equations for the 19 nodes, as shown in Fig. 2, can be obtained, with a general form for the ith node as,

$$\frac{\mathrm{d}}{\mathrm{dt}}\left(\frac{T_i+T_{i+1}}{2}\right) = \frac{A_i}{M_i \cdot Cp_i}\left[q_{src} + \frac{T_{i-1}-T_i}{R_{i-1}\left(\frac{T_{i-1}+T_i}{2}\right)} - \frac{T_i-T_{i+2}}{R_i\left(\frac{T_i+T_{i+1}}{2}\right)+R_{i+1}\left(\frac{T_{i+1}+T_{i+2}}{2}\right)}\right] \ (i = 1,2 \ldots 19) \quad \text{(Eq. 18)}$$

The pool boiling heat transfer occurs at the inner wall surface of the cryogenic vessel. The heat transfer equation can be formulated as,

$$\frac{\mathrm{d}T_i}{\mathrm{dt}} = \frac{A_i}{M_i \cdot Cp_i}\left[\frac{T_{i-1}-T_i}{R_{i-1}\left(\frac{T_{i-1}+T_i}{2}\right)} - q_{boil}\right] \ (i = 20) \quad \text{(Eq. 19)}$$

In Eq. 18 and Eq. 19, T_i is the material temperature as an independent variable, K; A_i the cross section area perpendicular to the heat flux, m^2; M_i the material mass, kg; Cp_i the specific heat capacity, J/kg/K; q_{src} the source of heat flux, W/m^2, which can be q_{dep} (Eq. 6), q_{conv} (Eq. 10) and/ or q_{rad} (Eq. 11) depending on where the node is; R_i the thermal insulance of the material, m^{2}K/W.

It should be noted that:

- The discretion form of the heat transfer equation can be different. The second term inside the square brackets of Eq. 18 vanishes for the first node (i=1).
- The "material" refers to one of the three, the MLI, the iced nitrogen or the stainless steel.
- The R_i depends not only on the temperature, but also on the vacuum pressure P_v for the nodes of the MLI, and also on the growing mass of deposition M_{sn} for the solid nitrogen node.
- The A_i increases with time for the solid nitrogen node, which is a function of both the material temperature and the deposited mass.
- The Cp_i varies with the temperature in the nodes of the iced nitrogen or the stainless steel.

The Eq. 18 and Eq. 19 together with Eq. 3 and Eq. 7 form a group of 22 ordinary differential equations (ODEs), with 22 independent variables, T_i (i=1,2,..20), P_v and M_{sn}. The closed group of equations can be solved by using a mathematical tool, e.g. MATHCAD, with support of the material properties.

5 CRYOGENIC MATERIAL PROPERTIES

The correctness of the ODEs' solutions is highly depending on the accurate material properties, which vary significantly with the cryogenic temperature. The thermal properties of the gaseous and solid nitrogen, the stainless steel and the MLI are carefully prepared to support the calculation.

The saturation density and pressure of nitrogen [10] are the key parameters to determine if mass deposits or not, as shown in Fig. 3 (left). The precise fitting to the very small values in the temperature range below the triple point (63 K) is essentially important to judge the desublimation criterion (Eq. 4), which are zoomed in a logarithmic scale, as shown in the top-left square in Fig. 3 (left). The enthalpies of solid

phase (below triple point) and liquid phase (above triple point) of nitrogen are one of the dominating parameters to determine the heat flux due to mass deposition (Eq. 6), as shown in Fig. 3 (right).

The thermal properties of gaseous nitrogen are shown in Fig. 4. As shown, they vary remarkably with the cryogenic temperatures and must be represented accurately in the convection model (Eq. 8-10) for a correct estimation.

The thermal properties of solid nitrogen as shown in Fig. 5, support the conduction model (Eq. 15-16). As shown in the figure, two sudden jumps occur on the curves of heat capacity and the density, respectively, when the temperature approaches the transition point from the crystal type α to β of nitrogen (about 35.6 K) [13,24] and to the triple point (63 K).

The thermal conductivity and the heat capacity of the stainless steel 316 [22] are shown as functions of cryogenic temperature in Fig. 6 (left), instead of constants in conventional temperature range. The two properties support the conduction model of steel (Eq. 17).

The apparent conductivity of the MLI materials is measured as data by the manufacturer [23]. It turns out to be a function of the vacuum pressure and the temperature as shown in Fig. 6 (right). The conductivity is computed by double interpolations on the two parameters for the conduction model of the MLI (Eq. 14).

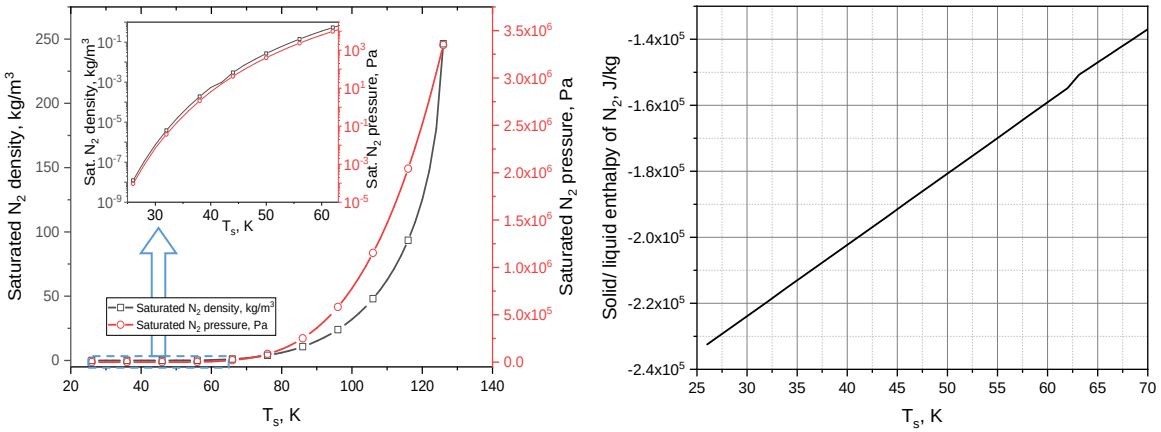

Figure 3. Saturation density, pressure and solid/ liquid enthalpy of nitrogen

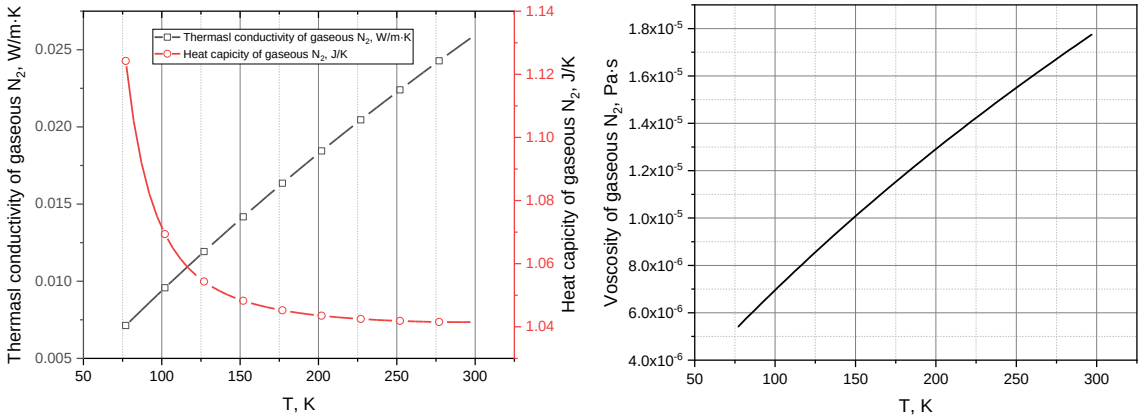

Figure 4. Thermal conductivity, heat capacity and dynamic viscosity of gaseous nitrogen

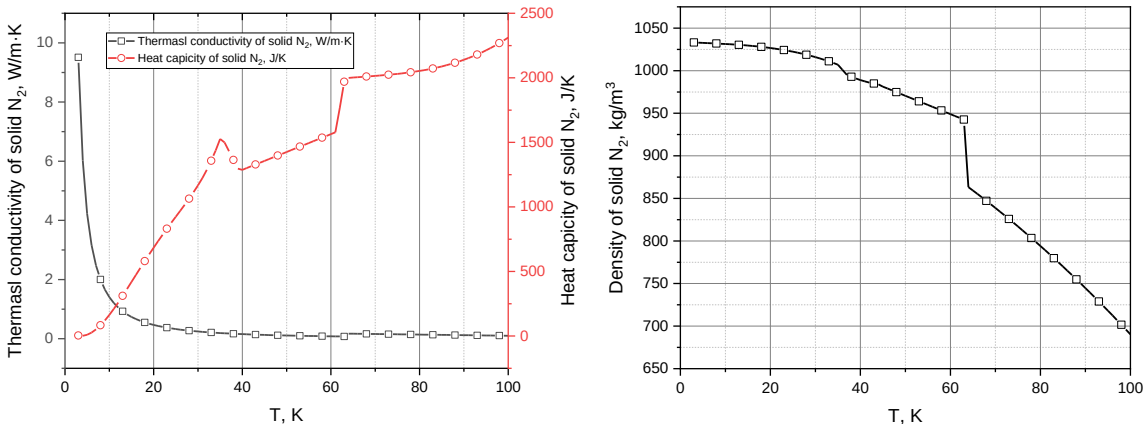

Figure 5. Thermal conductivity, heat capacity and density of iced nitrogen

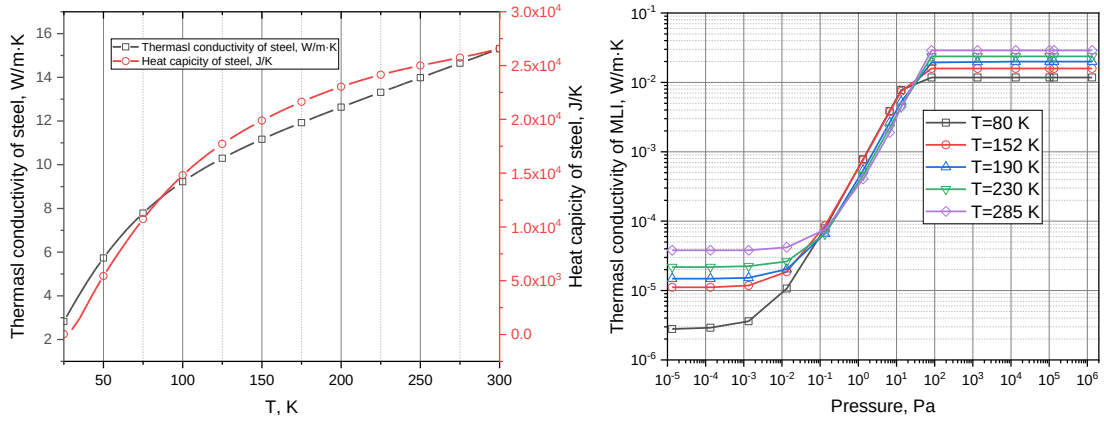

Figure 6. Thermal conductivity of heat capacity of stainless steel 316 and thermal conductivity of the MLI

6 COMPUTATION RESULTS

With the support of the material properties, the group of ODEs are solved by using the MATHCAD. The transient parameters of the LH2 cryostat in the first 30 s in LOVA are obtained as the solutions.

With a given size of the break on the vacuum vessel wall, the vacuum pressure evolution along time is shown in Fig. 7a. It indicates that the pressurization is fast. It takes about 10 s for the pressure to increase to the 99% of the upper limit (ambient pressure).

The venting mass flow rate of nitrogen is shown in Fig. 7b. The critical flow rate remains constant up to 2.5 s, and then decays over time due to the decreasing pressure difference between the ambient and the vacuum enclosure. The mass deposition rate due to desublimation is shown in Fig. 7b, with the peak value at about 2 s. It is remarkable that quasi balance is set up between the mass source (venting flow) and the mass sink (desublimation) at about 10 s.

The heat fluxes due to mass deposition, convection and thermal radiation are depicted in Fig. 7c. It is obvious that the heat fluxes of convection and radiation are negligible compared to that of phase change of the venting gas, i.e. the thermal load due to mass deposition dominates the safety limit of the cryostat. The peak value of the heat flux to the LH2 is $1.67 \cdot 10^4$ W/m^2, namely, 1.67 W/cm^2, at t ≈ 3 s. In other similar studies, the measured q_{dep} ranges in 3 – 6 W/cm^2 for a LHe cryostat in LOVA with vacuum insulation only, and in 0.3 – 1.93 W/cm^2 with additional insulation of MLI or other shields [25-31].

The temperature evolutions at the different layers are shown in Fig. 7d. At the beginning stage of LOVA the temperatures increase remarkably in the MLI, in the solid nitrogen and in the stainless steel due to the ingress of the "warm" venting gas, before a slow evolution process is observed. At t = 30 s, the inner surface temperature of the stainless steel is 26.6 K. The pool boiling in the cryogenic vessel contributes to the 0.6 K temperature difference between the LH2 and the vessel wall. The outer surface temperatures of the steel wall, the solid nitrogen layer and the MLI is 34.7 K, 65.6 K and 128.7 K, respectively. Thus, the thermal resistances of the stainless steel, the solid nitrogen layer and the MLI contribute to the temperature differences of 8 K, 31 K and 63 K, respectively. The temperature drop in the solid nitrogen layer is almost half of that of the MLI, although the thickness of the iced nitrogen layer is in an order of half millimeter (Fig. 7e), only a tiny fraction of the MLI thickness. It means the solid nitrogen itself is a good thermal insulation material, due to its very low thermal conductivity.

The surface temperature of the nitrogen layer after t = 5 s is higher than the nitrogen triple point (63 K) by within 2.5 K. In this condition, condensation takes place.

The growing processes of the solid nitrogen layer and the total deposited mass are shown in Fig. 7e. At t = 30 s, the solid nitrogen layer thickness reaches 0.54 mm and the total deposited mass of nitrogen is about 0.7 kg.

The heat fluxes due to convection and thermal radiation, which are 67 W/m^2 and 27 W/m^2, respectively, at the later equilibrium stage, are shown together in Fig. 7f for comparison. They occupy only 0.14% and 0.36%, respectively, of the peak thermal load caused by the mass deposition. Therefore, the two phenomena are ignored in some similar studies [1-3].

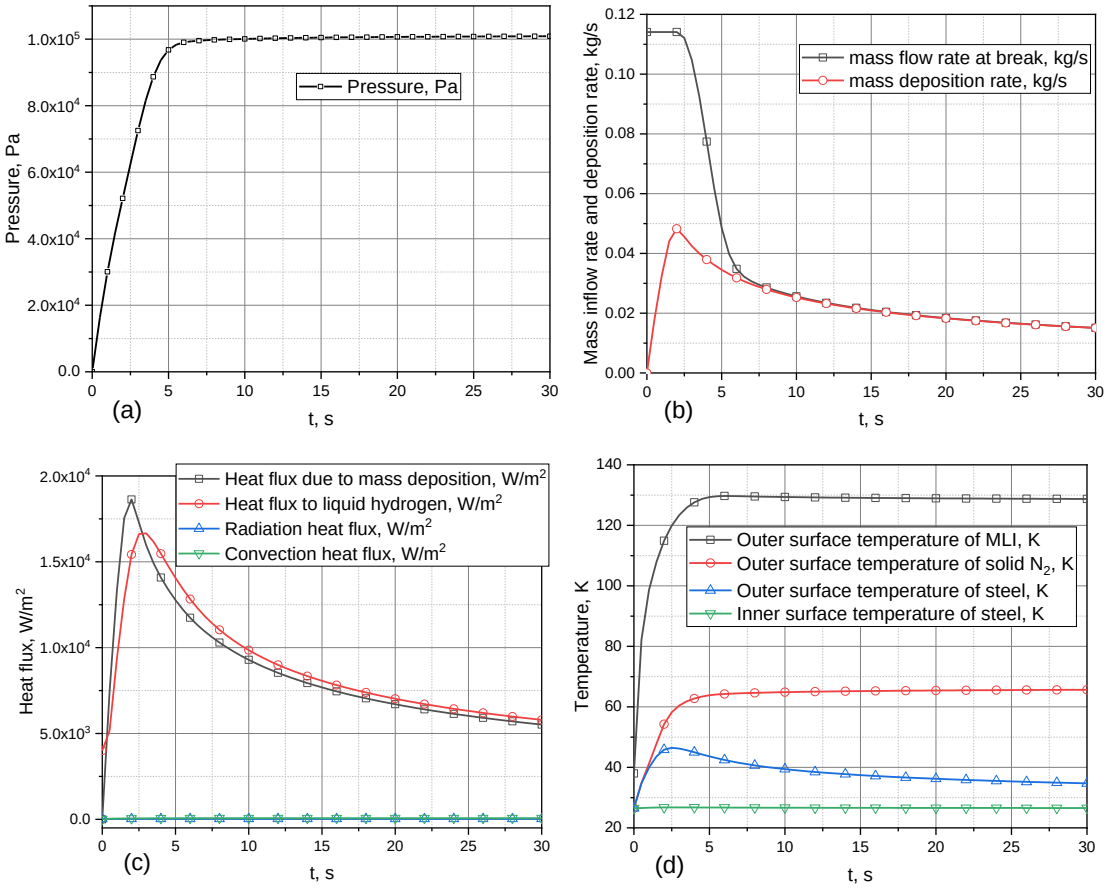

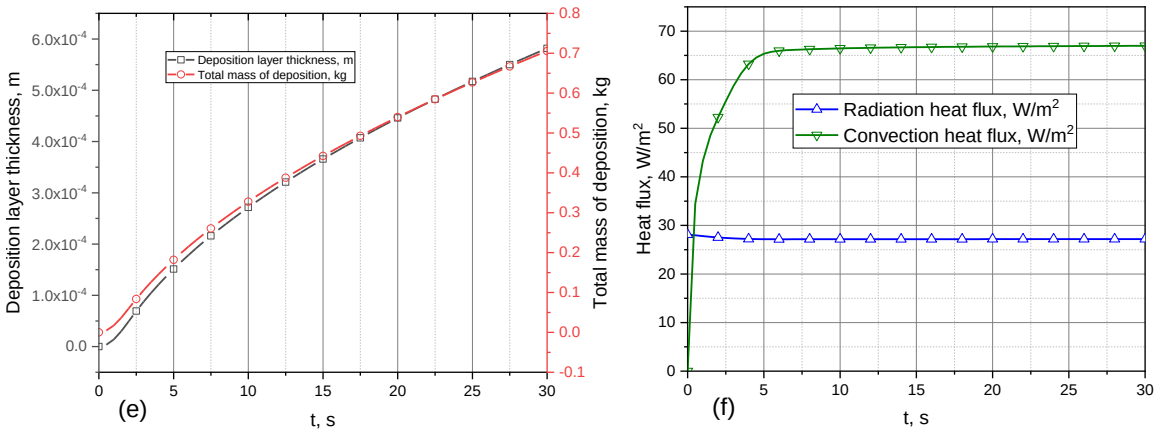

Figure 7. Transient parameter evolutions in the LH2 cryostat in the first 30 s in a LOVA

7 CONCLUSIONS

Zero dimensional lumped parameter models on heat and mass transfers are developed to find the thermal load to the LH2 cryostat in a loss of vacuum accidental (LOVA) scenario, by modelling the multi-layer insulation, the iced nitrogen layer, the convection in the vacuum enclosure and the pool boiling heat transfer in the cryogenic vessel. Due to the difficulty of determining the actual location of nitrogen deposition, the nitrogen gas is assumed conservatively to desublimate on the outer surface of the cryogenic vessel wall. The computed results confirm that the mass deposition dominates the contributions to the thermal loads to the LH2. The convection and thermal radiation play significantly less roles. The estimated heat flux to the LH2 in LOVA supplies a key input parameter for the safety valve design for the cryogenic vessel. The computed thermal-dynamic parameters in the LH2 cryostat system support the design of the experimental facility for LOVA tests, including the cryostat itself and the auxiliary measuring system. In turn, the test data will be used to verify the theoretical models in future work.

ACKNOWLEDGMENT

The research is financially supported by the Airbus Operations GmbH, Hamburg, which is appreciated by the authors for the funding support.

REFERENCES

1. Zoller C, Experimental Investigation and Modelling of Incidents in Liquid Helium Cryostats, Dissertation KIT, May 2018
2. Heidt C, Grohmann S and Süßer M, Modeling the pressure increase in liquid helium cryostats after failure of the insulating vacuum, AIP Conference Proceedings 1573, 1574 (2014); https://doi.org/10.1063/1.4860894, Published Online: 17 February 2015
3. Weber C, Henriques A and Grohmann S, Study on the heat transfer of helium cryostats following loss of insulating vacuum, IOP Conf. Series: Materials Science and Engineering 502 (2019) 012170, doi:10.1088/1757-899X/502/1/012170
4. Parma V, Cryostat Design, CERN, Geneva, Switzerland
5. Kutateladze S S 1951 Izvestia Akademia Nauk Otdelenie Tekhnicheski Nauk 4 529-536
6. Breen B P and Westwater J W, Effect of diameter of horizontal tubes on film heat transfer, Chem. Eng. Prog. 58(7), 67, 1962
7. Bewilogua L, Knöner R and Vinzelberg H, Heat transfer in cryogenic liquids under pressure, Cryogenics, Volume 15, Issue 3, March 1975, Pages 121-125

8. Hilal M A and Boom R W, An experimental investigation of free convection heat transfer in supercritical helium, International Journal of Heat and Mass Transfer, Volume 23, Issue 5, May 1980, Pages 697-705
9. Fesmirea J E, Johnson W L, Cylindrical cryogenic calorimeter testing of six types of multilayer insulation systems, Cryogenics 89 (2018) 58–75
10. Lemmon E W, Huber M L and McLinden M O, Reference Fluid Thermodynamic and Transport Properties (REFPROP), NIST Standard Reference Database 23, Version 8.0, National Institute of Standards and Technology (NIST), USA
11. Xie G F, Li X D, Wang R S, Study on the heat transfer of high-vacuum-multilayer-insulation tank after sudden, catastrophic loss of insulating vacuum, Cryogenics, Volume 50, Issue 10, October 2010, Pages 682-687 http://dx.doi.org/10.1016/j.cryogenics.2010.06.020
12. Masae Kanda, Kazuaki Matsumoto, Sataro Yamaguchi, Heat transfer through multi-layer insulation (MLI), Physica C: Superconductivity and its applications 583 (2021) 1353799
13. Scott T A, Solid and liquid nitrogen, Physics Reports (Section C of Physics Letters) 27, No. 3, 85 - 157. North-holland Publishing Company, 1976
14. Daniel Brewer G, Hydrogen Aircraft Technology, ISBN 0-8493-5838-8, TL704.7.B65 1991, International Standard Book Number 0-8493-5838-8 Library of Congress Card Number 90-47972 Printed in the United States
15. Silberhorn D, Atanasov G, Walther J-N, Zill T, Assessment of hydrogen fuel tank integration at aircraft level, Provided by Institute of Transport Research: Publications
16. McCarty R D, Hord J, Roder H M, Selected Properties of Hydrogen, Engineering Design Data, US Department of Commerce, Malcolm Baldrige, Secretary National Bureau of Standards, Feb. 1981
17. Al Ghafri S Z S, Swanger A, Jusko V, Siahvashi A, Perez F, Johns M L, May E F, Modelling of Liquid Hydrogen Boil-Off, Energies 2022, 15, 1149. https://doi.org/10.3390/en15031149
18. Weber C et al, Safety studies on vacuum insulated liquid helium cryostats, 2017 IOP Conf. Ser.: Mater. Sci. Eng. 278 012169
19. https://www.flukeprocessinstruments.com/en-us/service-and-support/knowledge-center/infrared-technology/emissivity-metals
20. Verein Deutscher Ingenieure 2010 VDI Heat Atlas 2nd ed (Springer)
21. https://en.wikipedia.org/wiki/Low_emissivity
22. Peter E. Bradley and Ray Radebaugh, Properties of selected materials at cryogenic temperatures, National Institute of Standards and Technology (NIST), USA
23. https://www.lydallpm.com/products/low-temperature-insulation/crs-wrap-super-insulating-media/product-sheets/
24. https://en.wikipedia.org/wiki/Solid_nitrogen
25. Lehmann W, and Zahn G, Proc. Int. Cryog. Eng. Conf. 7, 569–579 (1978)
26. Cavallari G, Gorin I, Güsewell D, and Stierlin R, Proc. 4th Workshop on RF Supercon. 1, 781–803 (1989)
27. Harrison S M, IEEE T. Appl. Supercon. 12, 1343–1346 (2002), ISSN 1051-8223
28. Bartenev V D, Dadskov V I, Shishov Y A, and Zel'dovich A G, Cryogenics 26, 293–296 (1986)
29. Ercolani E, Gauthier A, Gully P, and Poncet J, Quantification of heat flux in supercritical helium, Presentation at the 1st Cryogenic Safety – HSE Seminar at CERN (2016), URL https://indico.cern.ch/event/495194/contributions/2181322/
30. Dhuley R C, and Sciver S W V, IOP Conf. Ser.: Mater. Sci. Eng. 101, 012006 (2015)
31. Dhuley R C, and Sciver S W V, IEEE T. Appl. Supercon. 25, 1–5 (2015), ISSN 1051-8223
32. Neumann T A, Albert M R, Lomonaco R, Engel C, Courville Z, Perron F, Experimental determination of snow sublimation rate and stable-isotopic exchange, Annals of Glaciology 49, 2008, https://doi.org/10.3189/172756408787814825 Published online by Cambridge University Press